Applied Catalysis B: Environmental 331 (2023) 122691

Contents lists available at ScienceDirect

Applied Catalysis B: Environmental

journal homepage: www.elsevier.com/locate/apcatb

Substoichiometric covalent organic frameworks with uncondensed aldehyde for highly efficient hydrogen peroxide photosynthesis in pure water

Yong Liu [a], Wang-Kang Han [a], Wenwen Chi [a], Yuqian Mao [a], Yuqin Jiang [b], Xiaodong Yan [a], Zhi-Guo Gu [a,*]

[a] Key Laboratory of Synthetic and Biological Colloids, Ministry of Education, School of Chemical and Material Engineering, Jiangnan University, Wuxi 214122, China
[b] Henan Engineering Research Centre of Chiral Hydroxyl Pharmaceutical, School of Chemistry and Chemical Engineering, Henan Normal University, Xinxiang 453007, China

ARTICLE INFO

Keywords:
Covalent organic frameworks
Substoichiometric
Uncondensed aldehyde
Hydrogen peroxide photosynthesis
bex topology

ABSTRACT

A substoichiometric covalent organic framework (Bpy-TAPT) with reserved polar aldehyde groups and dual active sites (bipyridine and triazine) was rationally designed for recorded photocatalytic production of H_2O_2 in pure water. Bpy-TAPT showed an unprecedented H_2O_2 production rate of 4038 μmol h^{-1} g^{-1} with no sacrificial agents or cocatalysts, exceeding all the previously reported COF-based photocatalysts. Both experimental and computational results suggested that the dual active sites widened the visible-light-responsive range of the catalyst as well as enhanced the charge generation, while the aldehyde groups with electron-rich properties effectively improved the separation of carriers and the adsorption of O_2/H^+. This substoichiometric strategy suggests a powerful polarization method for the development of highly efficient photocatalysts in artificial photosynthesis.

1. Introduction

Hydrogen peroxide (H_2O_2) is one of the most valuable oxidants with widespread applications in healthcare, chemical industries and water treatment [1–4]. The market demand for H_2O_2 may increase to 5.7 million tons per annum by 2027 [5–7]. Anthraquinone oxidation is the common method for industrial H_2O_2 production, though it consumes a lot of energy and generates hazardous waste [8,9]. Artificial photosynthesis of H_2O_2 through a 2-electron oxygen reduction pathway ($2e^-$ ORR, $O_2 + 2e^- + 2H^+ \rightarrow H_2O_2$) from water and oxygen using semiconductor photocatalysts has attracted attention because of its green, environmentally friendly and energy saving characters [10–12]. Specifically, metal-free polymeric semiconductors exhibit low activity for H_2O_2 decomposition compared to metal-based inorganic semiconductors, which are very promising candidates as low-cost and sustainable photocatalysts for solar-driven H_2O_2 production [13–16].

Covalent organic frameworks (COFs) are a new type of crystalline semiconductors for photocatalytic H_2O_2 production, whose energy bands and reactive sites can be adjusted at the molecular level [9,17,18]. Nevertheless, the reported strategies on developing COFs toward photosynthetic H_2O_2 are generally through integrating conjugated building blocks [19,20]. On the one hand, these promising COFs suffer from the tedious and laborious synthesis, and the insufficient active sites for photocatalysis. On the other hand, COFs still suffer from the intramolecular charge recombination due to the diverse symmetry of their periodic structures. Therefore, it is very urgent to develop an innovative molecular engineering strategy to precise construction of COFs containing sufficient redox sites and facilitate charge separation for efficient H_2O_2 generation in pure water.

The conjugated high-nitrogen-content triazine and bipyridine moieties with high electron affinity exhibit remarkable electronic and optical behavior [21]. On the other hand, the engineering of polar groups (e.g., oxygen groups, halogen) is a promising route to radically facilitate charge separation of polymer semiconductors [22]. With in this mind, a combined strategy was rationally designed by introducing dual active sites of bipyridine and triazine in substoichiometric COF with reserved polar aldehyde groups (Scheme 1), can significantly enhance the photocatalytic performance toward photosynthesis of H_2O_2 in pure water. This special COF named Bpy-TAPT has the following advantages for H_2O_2 photosynthesis: (1) Bipyridine and triazine provide sufficient

* Corresponding author.
E-mail address: zhiguogu@jiangnan.edu.cn (Z.-G. Gu).

https://doi.org/10.1016/j.apcatb.2023.122691
Received 13 December 2022; Received in revised form 14 February 2023; Accepted 23 March 2023
Available online 24 March 2023

generation sites of photogenerated electrons and holes, as well as 2e⁻ ORR reaction sites; (2) Reserved polar aldehyde groups increase the adsorption of O_2/H^+ to enhance the production of H_2O_2 in 2e⁻ ORR reduction; (3) The aldehyde groups with electron-rich properties effectively improve the separation of electrons and holes from triazines and bipyridines respectively, thereby increasing the photocatalytic efficiency. Consequently, Bpy-TAPT exhibited a much higher photocatalytic H_2O_2 production rate (4038 μmol h^{-1} g^{-1}) than that of Bpy-TAPB (2064 μmol h^{-1} g^{-1}) with single active sites and Bpy-TAPT-CN (1910 μmol h^{-1} g^{-1}) without reserved aldehyde in pure water, which is the highest value in recently reported COF-based photocatalysts for photosynthesis of H_2O_2. Moreover, this is the first report of substoichiometric COFs toward photosynthetic H_2O_2, and the combined strategy of reserving polar groups with dual active sites provides novel thoughts for the designing of highly efficient organic polymer photocatalysts.

2. Experimental

A complete description of chemicals, materials, and instrumentations is available in the Supporting Information.

2.1. Synthesis of Bpy-TAPT and Bpy-TAPB

A Pyrex tube of 20 × 60 mm (o.d × length) was charged with Bpy (16.8 mg, 0.04 mmol), TAPT (21.24 mg, 0.06 mmol for Bpy-TAPT) or TAPB (21.06 mg, 0.06 mmol for Bpy-TAPB), 1-Butanol (0.2 mL), and 1, 2-Dichlorobenzene (1.8 mL). After sonication for 10 min, 0.2 mL of aqueous acetic acid (6 M) was added and sonicated for 10 min. The tube was flash frozen at 77 K (liquid N_2 bath), evacuated to an internal pressure of 50 mTorr and flame sealed. The reaction was heated at 120 °C for 72 h yielding yellow solids at the bottom of the tube which was isolated by centrifugation and washed with DMF. Then solids were transferred to a Soxhlet extractor and washed with THF (24 h). Finally, the product was evacuated at 120 °C under vacuum overnight to obtain yellow powder. Yield: 75 %. Elemental analysis of Bpy-TAPT: Calcd. for $C_{94}N_{16}O_2H_{56}$: C, 78.33 %; N, 15.56 %; O, 2.22 %; H, 3.89 %. Elemental analysis of Bpy-TAPB: Calcd. for $C_{100}N_{10}O_2H_{62}$: C, 83.68 %; N, 9.76 %; O, 2.24 %; H, 4.32 %.

2.2. Synthesis of Bpy-TAPT-CN

The as-prepared Bpy-TAPT (30 mg) was dispersed in DMF (15 mL) with malononitrile (30 mg) and triethylamine (20 mg) by sonication for 10 min. The mixture was kept stirring for 24 h at 70 °C. The resulting solid was isolated by filtration and washed with DMF. Finally, the product was evacuated at 120 °C under vacuum overnight to obtain yellow powder. Yield: 87 %. Elemental analysis of Bpy-TAPT-CN: Calcd. for $C_{100}N_{20}H_{56}$: C, 78.13 %; N, 18.23 %; H, 3.64 %.

2.3. Photocatalytic H_2O_2 production

5 mg of photocatalyst and 30 mL of water were introduced into a hermetically sealed device, a quartz tube with a cap. The suspending solution was well distributed by ultrasonication for 30 min and O_2 was blown into the suspension. The suspension was stirred in the dark for 30 min to reach the adsorption-desorption balance before the photocatalytic test was performed. A 300 W Xenon lamp source (PLS-SEX 300, Beijing Perfectlight Co., Ltd, China) was used as the light source ($\lambda > 420$ nm, 100 mW cm^{-2}). The concentration of H_2O_2 was determined by the potassium titanium oxalate method, where 1.5 mL of the solution was drawn from the reactor using a syringe with a 4 μm filter at a given time interval and then mixed with 1 mL of a 0.02 M potassium titanium oxalate solution. The solution then changed from transparent to yellow due to the formation of Ti peroxides. The absorbance at 400 nm was used to determine the concentration of H_2O_2 and monitored by a UV-Vis spectrometer.

3. Results

3.1. Characterization of Bpy-COFs

Bpy-TAPT and Bpy-TAPB were synthesized by Bpy as tetratopic linkers with TAPT or TAPB as tritopic linkers respectively, and Bpy-TAPT-CN was obtained via Knoevenagel condensation (Fig. 1a, S5-S6). The remarkable vibration band at 1620 cm^{-1} with the disappearance of the $-NH_2$ stretching bands (3250–3450 cm^{-1}) in FT-IR spectra indicates the generation of C=N (Fig. 1d, S7). Notably, the retained C=O stretching band at 1690 cm^{-1} proves the uncondensed aldehyde groups in Bpy-TAPB and Bpy-TAPT. For Bpy-TAPT-CN, the stretching vibration of C=O disappeared and meanwhile the new band appeared at 2200 cm^{-1}, corresponding to C≡N, indicated the successful condensation of malononitrile [23,24]. These results were further confirmed by ^{13}C NMR spectroscopy (Fig. S8-S10). A typical peak at around 155 ppm was observed in Bpy-TAPB and Bpy-TAPT, confirming the imine condensation, while the residual aldehyde groups were also observed at 192 ppm. Furthermore, the signals at 115 ppm in Bpy-TAPT-CN belong to the carbon atoms in the C≡N units [25].

The crystal structure of Bpy-TAPT, Bpy-TAPB and Bpy-TAPT-CN were determined by powder X-ray diffraction (PXRD) measurement in conjunction with structural simulations (Fig. 1e, S11). As the three COFs

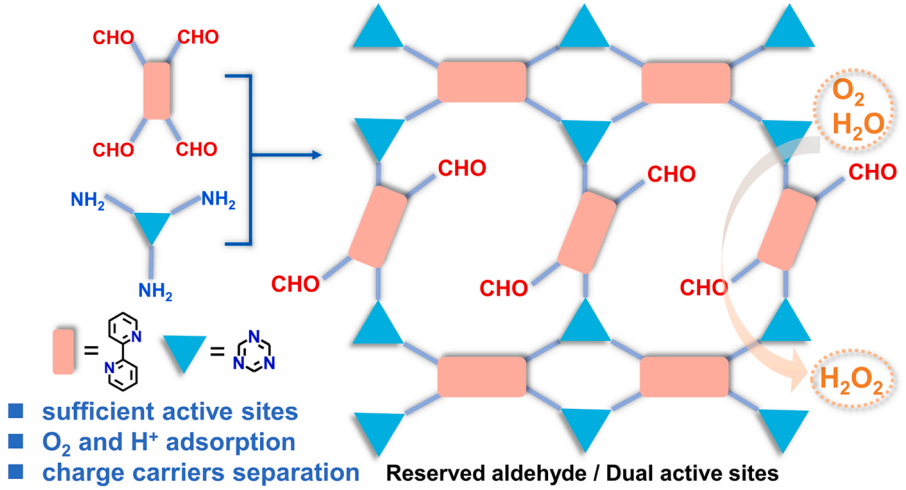

Scheme 1. Substoichiometric COFs with reserved aldehyde and dual active sites for highly efficient H_2O_2 photosynthesis.

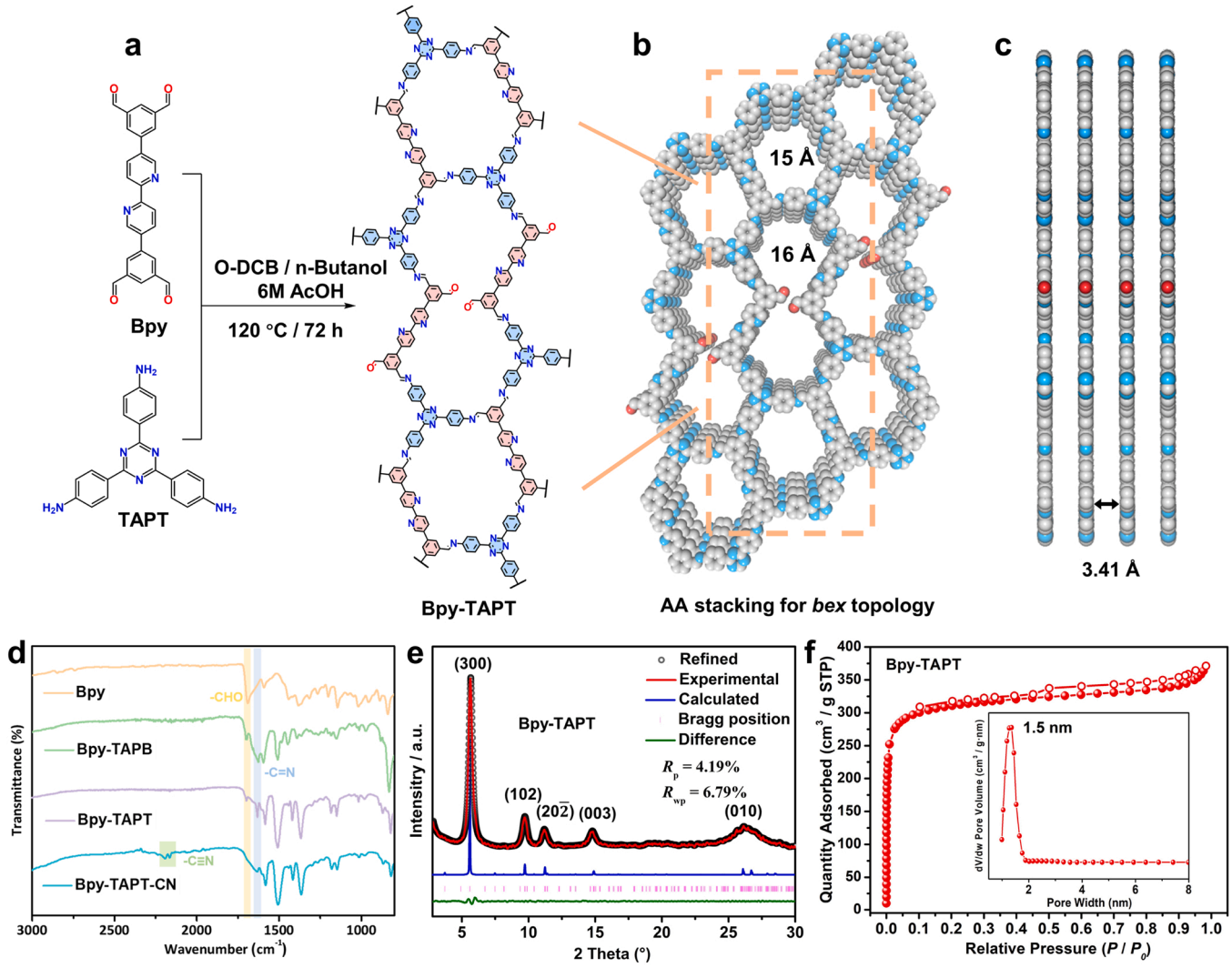

Fig. 1. (a) Synthesis and molecular structure of Bpy-TAPT. (b) Top view and (c) side view of the structure of Bpy-TAPT. (d) FT-IR spectrum of Bpy and the three COFs. (e) PXRD of Bpy-TAPT. (f) N_2 adsorption/desorption isotherms with the pore size distribution of Bpy-TAPT.

have the same topology, Bpy-TAPT is selected as an example to illustrate the unique structure. Bpy-TAPT exhibits an intense peak at 5.61°, and relatively weak peaks at 9.78°, 11.23°, and 14.88°. Notably, a broad stacking reflection can be seen at 26.11° ((010) crystal facet), indicating the formation of 2D COF [26–28]. Considering the geometry of the precursors and the connection patterns, only *bex* and *tth* nets for Bpy-TAPT are possible according to RCSR [29]. However, the mismatched length of Bpy forbids the formation of the closed ring of *tth* topology (Fig. S12) [30]. The simulation clearly suggested that Bpy-TAPT adopted an AA stacked *bex* topology (Fig. S13-S15). Finally, a full profile Pawley refinement was performed to obtain the unit cell parameters (a = 47.90 Å, b = 3.41 Å, c = 18.15 Å, $\alpha = \gamma = 90°$, $\beta = 79.20°$; R_p = 4.19 %, R_{wp} = 6.79 % for Bpy-TAPT). Fig. 1b showed that Bpy-TAPT was composed of one fully enclosed pore about 15 Å and another semi-closed pore about 16 Å which divided by reserved aldehyde, which formed a 2D AA stacking structure with layer spacing of 3.41 Å (Fig. 1c). Specifically, the triangular linkers TAPT connect two Bpy molecules at two points on both sides to produce a ribbon-like architecture (Fig. S16). The free -NH_2 termini of triangular linkers are then interconnected by Bpy molecule by its diagonal aldehyde groups, which acts as linear ditopic linker. Consequently, two uncondensed -CHO groups per unit cell were confirmed by FT-IR and ^{13}C NMR.

The three COFs showed excellent chemical and thermal stability. After being immersed in various solvents for 72 h, including EtOH, DMF, THF, 6 M NaOH and 6 M HCl (Fig. S17-S19), they retained their original structure and crystallinity without weight lose. Thermogravimetric analysis revealed that the frameworks are thermally stable up to 510 °C with slight weight loss (Fig. S20). Scanning electron microscopy (SEM) images revealed that all the three COFs present as nanometer-sized crystalline particles ranging from 50 to 100 nm. The transmission electron microscopy (TEM) showed 2D lamellar structure (Fig. S21-S23). Energy-dispersive spectroscopy (EDS) mapping exhibited that the three COFs were comprised of C, N and O (Fig. S24).

The N_2 adsorption−desorption isotherms of Bpy-TAPT (Fig. 1f) exhibit a type-I isotherm with a sharp adsorption at low pressure, demonstrating the presence of micropores. The Brunauer−Emmett−-Teller (BET) surface area is calculated to be 1225 $m^2\ g^{-1}$, which was higher than those of Bpy-TAPB and Bpy-TAPT-CN (Fig. S25-S26). For all the three COFs, the distribution of pore size was centered at 1.5 nm, which matched well with the theoretical structure and further confirmed their high crystallinity.

3.2. Photocatalytic hydrogen peroxide evolution reaction

Compared to Bpy-TAPB, both Bpy-TAPT and Bpy-TAPT-CN exhibit a wider visible light absorption spectrum with narrowed bandgaps (Fig. 2a). The corresponding Tauc's plots analysis from the Ultraviolet–visible spectra exhibited optical energy band gaps (E_g) of 2.56,

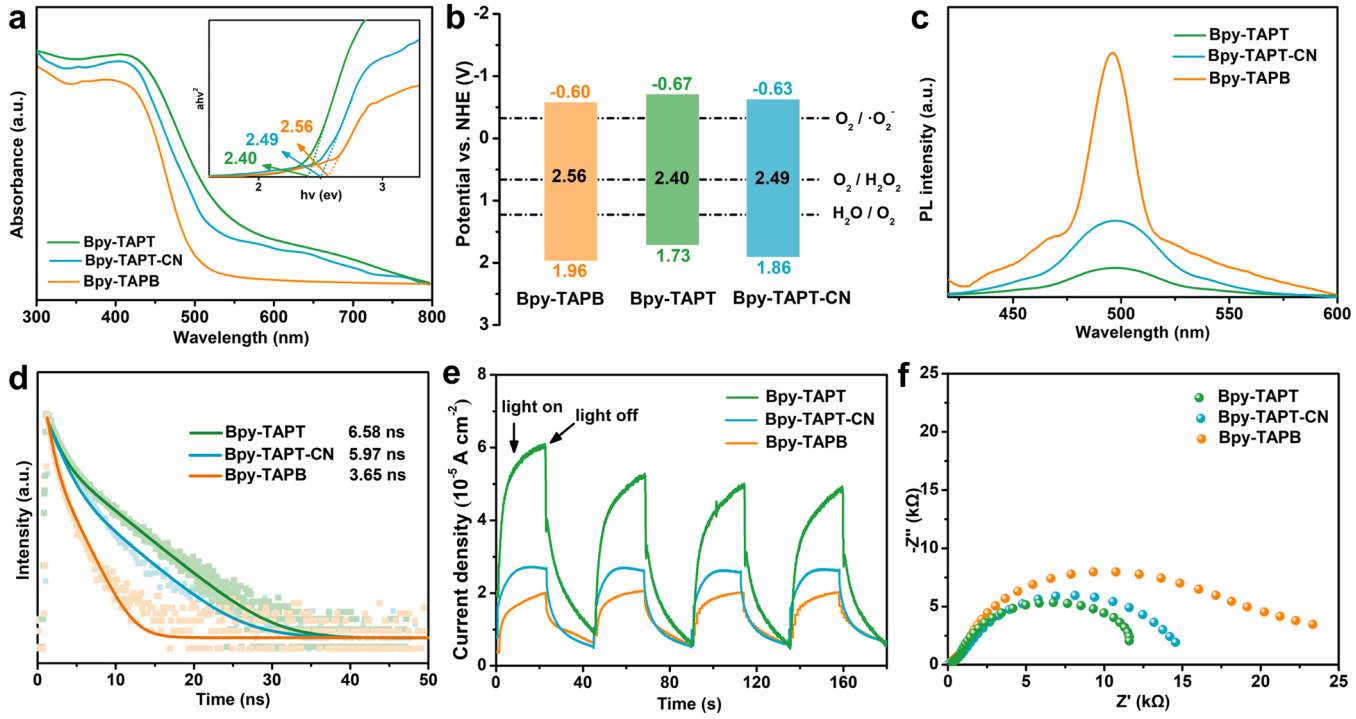

Fig. 2. (a) UV–vis spectra and Tauc plots of three COFs. (b) Electronic band structure of three COFs. (c) PL spectra with the excitation wavelength at 405 nm of three COFs. (d) Time-resolved PL decay curves of three COFs. (e) Transient photocurrents of three COFs. (f) Nyquist plots of three COFs.

2.40 and 2.49 eV for Bpy-TAPB, Bpy-TAPT and Bpy-TAPT-CN, respectively. According to the Mott–Schottky plots (Fig. S27-S29), the conduction band (E_{CB}) values were −0.60, −0.67 and −0.63 (V vs NHE) for Bpy-TAPB, Bpy-TAPT and Bpy-TAPT-CN, respectively. Based on the equation $E_g = E_{VB} - E_{CB}$, the VB positions of Bpy-TAPB, Bpy-TAPT and Bpy-TAPT-CN were calculated to be 1.96, 1.73 and 1.86 (V vs NHE) [31–33]. The band structures of the three COFs were sufficient for the reduction of O_2 to $\bullet O_2^-$ and the oxidation of H_2O to O_2, making these COFs promising photocatalysts for H_2O_2 production (Fig. 2b) [11,34].

Bpy-TAPB displayed an intense fluorescence signal and was substantially reduced for Bpy-TAPT and Bpy-TAPT-CN (Fig. 2c). This indicated that introducing triazine moieties into Bpy-COF greatly enhanced

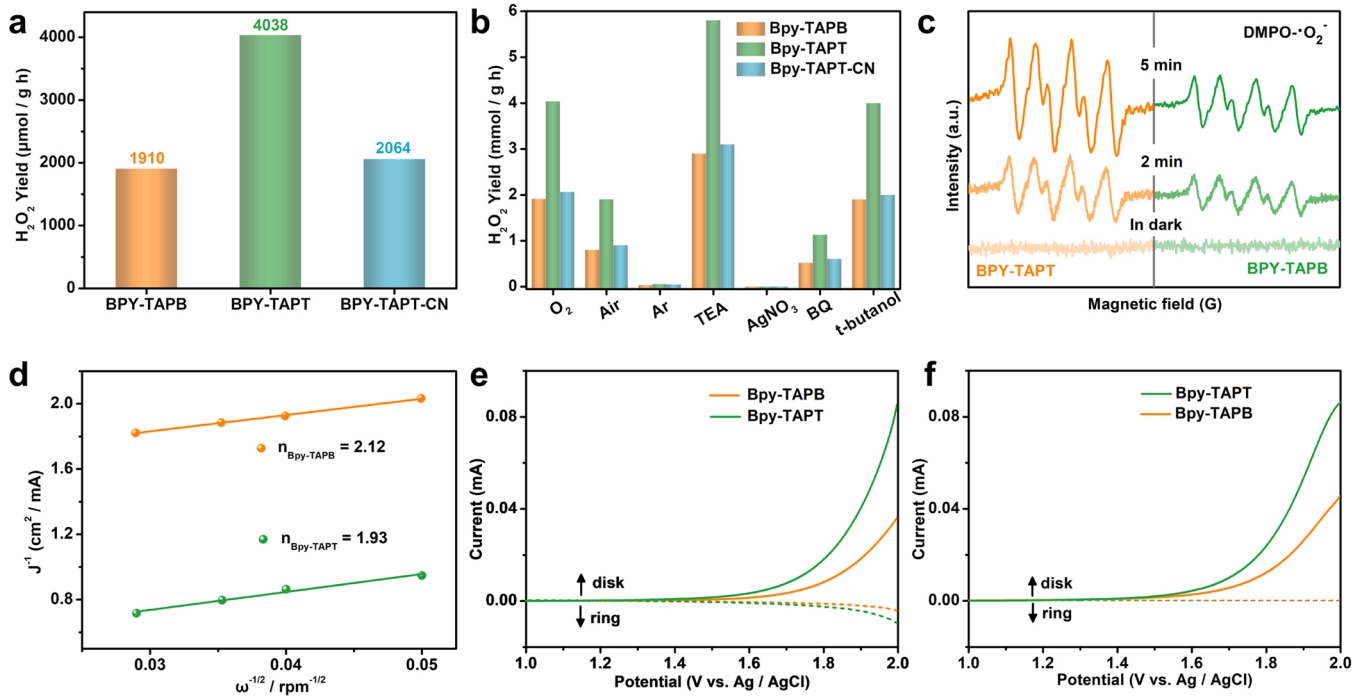

Fig. 3. (a) Photocatalytic production of H_2O_2 for three COFs. (b) Photosynthesis of H_2O_2 on three COFs under different reaction conditions. (c) The EPR spectra of Bpy-TAPT and Bpy-TAPB. (d) Koutecky–Levich plots obtained from RDE measurements. RRDE voltammograms: (e) The potential of Pt ring electrode was set at −0.23 V vs. Ag/AgCl to detect O_2. (f) The potential of Pt ring electrode was set at 0.6 V vs. Ag/AgCl to detect H_2O_2.

charge separation, which leaded to increased charge carrier lifetimes for Bpy-TAPT (6.58 ns) and Bpy-TAPT-CN (5.97 ns), as compared to that for Bpy-TAPB (3.65 ns) (Fig. 2d). The long lifetimes of Bpy-TAPT may be attributed to the electron-attracting properties of the uncondensed aldehyde, which retarded the recombination of photogenerated electrons with holes [35,36]. Futhermore, Bpy-TAPT showed the highest photocurrent density in transient photocurrents (Fig. 2e) and the photovoltage intensity in surface photovoltage (SPV) (Fig. S30), as well as the smallest impedance (Fig. 2f), which indicated the high charge separation efficiency and charge transfer kinetics [37,38].

Surprisingly, Bpy-TAPT exhibited an unprecedented H_2O_2 photocatalytic production rate of 4038 μmol h^{-1} g^{-1} without sacrificial reagents and stabilizers (Fig. 3a, S31), which is substantially higher than all the previously reported COF-based photocatalysts (Table S2). For comparison, the H_2O_2 production rates of Bpy-TAPB and Bpy-TAPT-CN were 1910 and 2064 μmol h^{-1} g^{-1}, respectively, which proved that the dual active sites and the reserved aldehyde sites were conducive to the generation of H_2O_2. The calculated apparent quantum yield (AQY) of Bpy-TAPT was 8.6 % at 420 nm, while the solar-to-chemical energy conversion (SCC) efficiency of Bpy-TAPT was 0.65 %. In addition, the H_2O_2 production rate (Fig. S32), FT-IR spectra and PXRD patterns of the three COFs were well maintained after several repeated cycles, suggesting good photocatalytic stability (Fig. S33). The three COFs exhibited deficient activity toward H_2O_2 decomposition under photoirradiation (Fig. S34). Furthermore, the organic dye RhB can be completely decomposed within 60 s by the produced H_2O_2 solution from Bpy-TAPT [39], while the ciprofloxacin solution can be decomposed in situ by self-Fenton reaction with Bpy-TAPT, where the decomposition rate exceeded 90 % within 40 min (Fig. S40) [40]. These results indicated Bpy-TAPT can be directly applied for photocatalytic treatment of environmental pollutants with excellent performance [41–43].

To investigate the photocatalytic H_2O_2 evolution mechanism over the three COFs, a series of experiments were performed. Bpy-TAPT, Bpy-TAPB and Bpy-TAPT displayed a contact angle of 35°, 65° and 75° respectively, demonstrated that reserved aldehydes could increase hydrophilicity (Fig. S35). The H_2O_2 production was greatly suppressed when switching O_2 atmosphere to air or Ar and completely disappearedadding when $AgNO_3$ was added to the reaction system, suggesting that the H_2O_2 was produced via the reduction of O_2 by electrons (Fig. 3b, S37). $^{18}O_2$ isotope experiments were further confirmed that the O_2 is essential for H_2O_2 production (Fig. S36). Also, the H_2O_2 yield was rapidly decreased after the addition of benzoquinone (BQ), indicated that $\bullet O_2^-$ was an essential intermediate for H_2O_2 generation. In contrast, the production of H_2O_2 was no declining with triethanolamine (TEA) and tert-butanol (TBA), proved that H_2O_2 was not generated directly by the photogenerated hole of Bpy-TAPT. The typical six characteristic signals for DMPO-$\bullet O_2^-$ were observed in Bpy-TAPB and Bpy-TAPT under light irradiation from electron paramagnetic resonance (EPR) (Fig. 3c), which intensity were increased with increasing illumination time and were absent in the dark, indicating the generation of $\bullet O_2^-$ intermediate. The average electron transfer numbers of ORR on Bpy-TAPB and Bpy-TAPT were measured by rotating disk electrode (RDE), which were 2.12 and 1.93, respectively (Fig. 3d, S38) [44]. Rotating ring-disk electrode (RRDE) exhibited a reduction current (dotted lines) due to the ORR at the Pt ring electrode when a constant potential of −0.23 V was applied to the Pt ring electrode (Fig. 3e), suggested that Bpy-TAPB and Bpy-TAPT can generate O_2 via water oxidation [44,45]. In contrast, when the potential applied at the ring electrode changed to an oxidative potential of 0.6 V, no oxidation current was observed (Fig. 3f). Hence, the photogenerated holes can oxidize water to O_2, and then generate superoxide radical ($\bullet O_2^-$) from photogenerated electrons, which could be further detected with nitro blue tetrazolium (NBT) in Ar (Fig. S39) [34].

The in situ FT-IR spectrometry were used to further explore the photocatalytic process of Bpy-TAPT. As shown in Fig. 4a, the intensity of the signals at 935 cm^{-1} attributed to the O−O bonding and 1156 cm^{-1} due to $\cdot O_2^-$ got increased along with the increase in lighting time

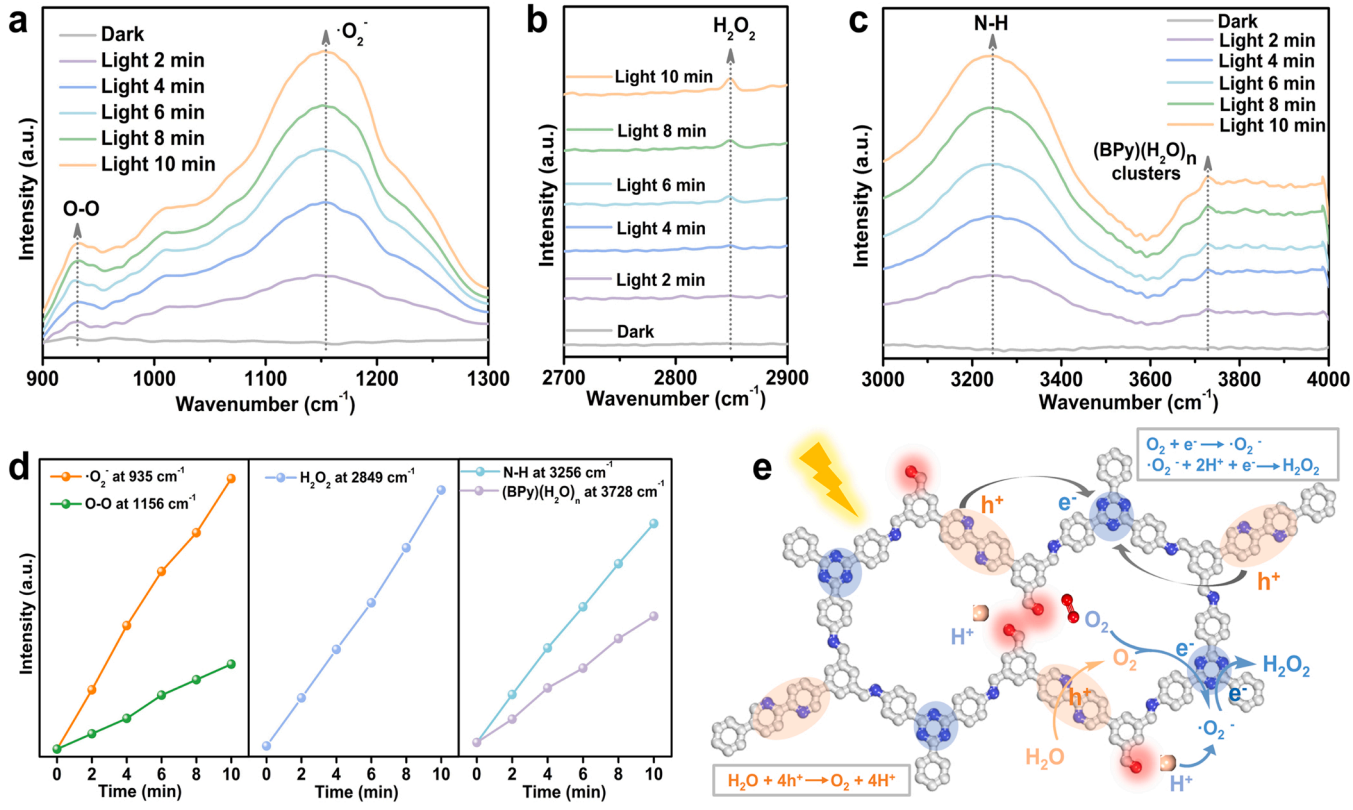

Fig. 4. In situ FT-IR spectra vs illumination time of Bpy-TAPT for photosynthetic H_2O_2 production at (a) 900–1300 cm^{-1}, (b) 2700–2900 cm^{-1} and (c) 3000–4000 cm^{-1}. (d) the intensity of the peaks at 935, 1156, 2849, 3256 and 3728 cm^{-1} vs illumination time. (e) Mechanism for photocatalytic H_2O_2 production of Bpy-TAPT.

(Fig. 4d), confirming the formation of superoxide anion radical and the two-step single-electron route [46,47]. The peak at 2849 cm^{-1} was attributed to the typical $(\nu_2 + \nu_6)/2\nu_6$ OH bending feature of H_2O_2 and gradually increasing under photoirradiation, which directly confirmed the formation of H_2O_2 under photoirradiation (Fig. 4b and d) [44,48]. Furthermore, the signals at 3256 and 3728 cm^{-1} can be attributed to the N-H stretching vibration in Bpy and the appeared $(BPy)(H_2O)_n$ clusters and the intensity also increased with the increasing time in illumination (Fig. 4c and d) [21,49], suggesting that Bpy might be the potential sites for the oxidation of water to oxygen in the photocatalytic reaction. To further understand the catalytic mechanism of Bpy-TAPT, density functional theory (DFT) was calculated [50]. The highest occupied molecular orbital (HOMO) and lowest unoccupied molecular orbital (LUMO) of Bpy-TAPT were partly localized on the bipyridine and triazine, suggested that bipyridine and triazine were oxidative and reductive sites, respectively (Fig. S41) [51]. The reserved aldehyde with electron-absorbing property located between HOMO and LUMO, which would contribute to accelerate the separation of electron/hole. The electrostatic potential surfaces and H^+/O_2 adsorption energies were also calculated (Fig. S41-S43) [38,51], which showed that aldehyde with the most negative electrostatic potential would be the possible absorption sites of O_2 and H^+ in $2e^-$ ORR, thus leading to the enhanced adsorption performance of Bpy-TAPT, and finally making contribution to the enhanced H_2O_2 production activity through $2e^-$ ORR.

Based on the above experiments and theoretical calculations, the mechanism for H_2O_2 formation on Bpy-TAPT was showed in Fig. 4e. The photoexcitation of Bpy-TAPT by photons leaded to the localization of photogenerated e^- and h^+ at triazine and bipyridine, respectively. The $(BPy)(H_2O)_n$ clusters was formed and then h^+ oxidized H_2O to O_2 at bipyridine sites. Meanwhile, $2e^-$ ORR was occurred at triazine sites, which the e^- reduced O_2 to form a $\bullet O_2^-$ and then converted to H_2O_2 via another e^- reduction. The reserved aldehyde groups promoted the separation of e^- from h^+ as well as the adsorption of O_2 and H^+ on the catalyst surface, which promoted the conversion to H_2O_2.

4. Conclusions

In summary, a substoichiometric COF Bpy-TAPT with reserved aldehyde was rationally designed for efficient photocatalytic production of H_2O_2 in pure water. The bipyridine and triazine promoted light absorption and carrier generation, while the reserved aldehyde with unique electron-rich structure enhanced the separation of carrier and the adsorption of O_2 and H^+. Bpy-TAPT showed a recorded H_2O_2 yield rate of 4038 μmol h^{-1} g^{-1}, which exceeded all the reported COF-based photocatalysts, and furthermore allowed for the rapid degradation of organic pollutants. This substoichiometric strategy suggests more opportunities to design of high-performance polymeric photocatalysts via the in-situ polarization for artificial photosynthesis and environmental remediation.

CRediT authorship contribution statement

Yong Liu: Conceptualization, Methodology, Validation, Investigation, Writing–Original Draft, Review & Editing. **Wang-Kang Han:** Validation, Writing–Original Draft. **Wenwen Chi:** Resources, Investigation. **Yuqian Mao:** Investigation. **Yuqin Jiang:** Supervision. **Xiaodong Yan:** Writing – Review & Editing. **Zhi-Guo Gu:** Supervision, Project administration, Funding acquisition.

Declaration of Competing Interest

The authors declare that they have no known competing financial interests or personal relationships that could have appeared to influence the work reported in this paper.

Data availability

Data will be made available on request.

Acknowledgements

This work was supported by the National Natural Science Foundation of China (22075108, 21905116), the Natural Science Foundation of Jiangsu Province (BK20190614), and the Open Research Fund of School of Chemistry and Chemical Engineering, Henan Normal University.

Appendix A. Supporting information

Supplementary data associated with this article can be found in the online version at doi:10.1016/j.apcatb.2023.122691.

References

[1] Y. Sun, L. Han, P. Strasser, A comparative perspective of electrochemical and photochemical approaches for catalytic H_2O_2 production, Chem. Soc. Rev. 49 (2020) 6605–6631.
[2] C. Xia, Y. Xia, P. Zhu, L. Fan, H. Wang, Direct electrosynthesis of pure aqueous H_2O_2 solutions up to 20% by weight using a solid electrolyte, Science 366 (2019) 226–231.
[3] Y. Xia, X. Zhao, C. Xia, Z.Y. Wu, P. Zhu, J.Y.T. Kim, X. Bai, G. Gao, Y. Hu, J. Zhong, Y. Liu, H. Wang, Highly active and selective oxygen reduction to H_2O_2 on boron-doped carbon for high production rates, Nat. Commun. 12 (2021) 4225.
[4] S.C. Perry, D. Pangotra, L. Vieira, L.-I. Csepei, V. Sieber, L. Wang, C. Ponce de León, F.C. Walsh, Electrochemical synthesis of hydrogen peroxide from water and oxygen, Nat. Rev. Chem. 3 (2019) 442–458.
[5] Y. Xue, Y. Wang, Z. Pan, K. Sayama, Electrochemical and photoelectrochemical water oxidation for hydrogen peroxide production, Angew. Chem. Int. Ed. 60 (2021) 10469–10480.
[6] Y. Wang, G.I.N. Waterhouse, L. Shang, T. Zhang, Electrocatalytic oxygen reduction to hydrogen peroxide: from homogeneous to heterogeneous electrocatalysis, Adv. Energy Mater. 11 (2020), 2003323.
[7] H. Hou, X. Zeng, X. Zhang, Production of hydrogen peroxide by photocatalytic processes, Angew. Chem. Int. Ed. 59 (2020) 17356–17376.
[8] J.M. Campos-Martin, G. Blanco-Brieva, J.L. Fierro, Hydrogen peroxide synthesis: an outlook beyond the anthraquinone process, Angew. Chem. Int. Ed. 45 (2006) 6962–6984.
[9] W. Zhao, P. Yan, B. Li, M. Bahri, L. Liu, X. Zhou, R. Clowes, N.D. Browning, Y. Wu, J.W. Ward, Accelerated synthesis and discovery of covalent organic framework photocatalysts for hydrogen peroxide production, J. Am. Chem. Soc. 144 (2022) 9902.
[10] Y. Shiraishi, T. Takii, T. Hagi, S. Mori, Y. Kofuji, Y. Kitagawa, S. Tanaka, S. Ichikawa, T. Hirai, Resorcinol-formaldehyde resins as metal-free semiconductor photocatalysts for solar-to-hydrogen peroxide energy conversion, Nat. Mater. 18 (2019) 985–993.
[11] H. Cheng, J. Cheng, L. Wang, H. Xu, Reaction pathways toward sustainable photosynthesis of hydrogen peroxide by polymer photocatalysts, Chem. Mater. 34 (2022) 4259–4273.
[12] J. Barber, Photosynthetic energy conversion: natural and artificial, Chem. Soc. Rev. 38 (2009) 185–196.
[13] B. Liu, J. Du, G. Ke, B. Jia, Y. Huang, H. He, Y. Zhou, Z. Zou, Boosting O_2 reduction and H_2O dehydrogenation kinetics: surface N-hydroxymethylation of g-C_3N_4 photocatalysts for the efficient production of H_2O_2, Adv. Funct. Mater. 32 (2022), 2111125.
[14] X. Zhang, P. Ma, C. Wang, L. Gan, X. Chen, P. Zhang, Y. Wang, H. Li, L. Wang, X. Zhou, Unraveling the dual defect sites in graphite carbon nitride for ultra-high photocatalytic H_2O_2 evolution, Energy Environ. Sci. 15 (2022) 830–842.
[15] Y. Shiraishi, M. Matsumoto, S. Ichikawa, S. Tanaka, T. Hirai, Polythiophene-doped Resorcinol–Formaldehyde resin photocatalysts for solar-to-hydrogen peroxide energy conversion, J. Am. Chem. Soc. 143 (2021) 12590–12599.
[16] L. Chen, L. Wang, Y. Wan, Y. Zhang, Z. Qi, X. Wu, H. Xu, Acetylene and diacetylene functionalized covalent triazine frameworks as metal-free photocatalysts for hydrogen peroxide production: a new two-electron water oxidation pathway, Adv. Mater. 32 (2020), 1904433.
[17] W.-K. Han, H.-S. Lu, J.-X. Fu, X. Liu, X. Zhu, X. Yan, J. Zhang, Y. Jiang, H. Dong, Z.-G. Gu, Targeted construction of a three-dimensional metal covalent organic framework with spn topology for photocatalytic hydrogen peroxide production, Chem. Eng. J. 449 (2022), 137802.
[18] C. Krishnaraj, H. Sekhar Jena, L. Bourda, A. Laemont, P. Pachfule, J. Roeser, C. V. Chandran, S. Borgmans, S.M.J. Rogge, K. Leus, C.V. Stevens, J.A. Martens, V. Van Speybroeck, E. Breynaert, A. Thomas, P. Van Der Voort, Strongly reducing (diarylamino)benzene-based covalent organic framework for metal-free visible light photocatalytic H_2O_2 generation, J. Am. Chem. Soc. 142 (2020) 20107–20116.
[19] W. Zhao, P. Yan, B. Li, M. Bahri, L. Liu, X. Zhou, R. Clowes, N.D. Browning, Y. Wu, J.W. Ward, Accelerated synthesis and discovery of covalent organic framework photocatalysts for hydrogen peroxide production, J. Am. Chem. Soc. 144 (2022) 9902–9909.

[20] L. Liu, M.-Y. Gao, H. Yang, X. Wang, X. Li, A.I. Cooper, Linear conjugated polymers for solar-driven hydrogen peroxide production: the importance of catalyst stability, J. Am. Chem. Soc. 143 (2021) 19287–19293.
[21] M. Kou, Y. Wang, Y. Xu, L. Ye, Y. Huang, B. Jia, H. Li, J. Ren, Y. Deng, J. Chen, Y. Zhou, K. Lei, L. Wang, W. Liu, H. Huang, T. Ma, Molecularly engineered covalent organic frameworks for hydrogen peroxide photosynthesis, Angew. Chem. Int. Ed. 61 (2022), e202200413.
[22] H. Wang, C. Yang, F. Chen, G. Zheng, Q. Han, A crystalline partially fluorinated triazine covalent organic framework for efficient photosynthesis of hydrogen peroxide, Angew. Chem. Int. Ed. 61 (2022), e202202328.
[23] T. Sun, Y. Liang, Y. Xu, Rapid, ordered polymerization of crystalline semiconducting covalent triazine frameworks, Angew. Chem. Int. Ed. 61 (2022), e202113926.
[24] J. Xu, Y. He, S. Bi, M. Wang, P. Yang, D. Wu, J. Wang, F. Zhang, An olefin-linked covalent organic framework as a flexible thin-film electrode for a high-performance micro-supercapacitor, Angew. Chem. Int. Ed. 58 (2019) 12065–12069.
[25] S. Xu, Z. Liao, A. Dianat, S.W. Park, M.A. Addicoat, Y. Fu, D.L. Pastoetter, F. G. Fabozzi, Y. Liu, G. Cuniberti, M. Richter, S. Hecht, X. Feng, Combination of knoevenagel polycondensation and water-assisted dynamic michael-addition-elimination for the synthesis of vinylene-linked 2D covalent organic frameworks, Angew. Chem. Int. Ed. 61 (2022), e202202492.
[26] A.P. Cote, A.I. Benin, N.W. Ockwig, M. O'Keeffe, A.J. Matzger, O.M. Yaghi, Porous, crystalline, covalent organic frameworks, Science 310 (2005) 1166–1170.
[27] M. Liu, Y.J. Chen, X. Huang, L.Z. Dong, M. Lu, C. Guo, D. Yuan, Y. Chen, G. Xu, S. L. Li, Y.Q. Lan, Porphyrin-based COF 2D materials: variable modification of sensing performances by post-metallization, Angew. Chem. Int. Ed. 61 (2022), e202115308.
[28] Z. Mi, T. Zhou, W. Weng, J. Unruangsri, K. Hu, W. Yang, C. Wang, K.A.I. Zhang, J. Guo, Covalent organic frameworks enabling site isolation of viologen-derived electron-transfer mediators for stable photocatalytic hydrogen evolution, Angew. Chem. Int. Ed. 60 (2021) 9642–9649.
[29] M. O'Keeffe, M.A. Peskov, S.J. Ramsden, O.M. Yaghi, The reticular chemistry structure resource (RCSR) database of, and symbols for, crystal nets, Acc. Chem. Res. 41 (2008) 1782–1789.
[30] B. Zhang, H. Mao, R. Matheu, J.A. Reimer, S.A. Alshmimri, S. Alshihri, O.M. Yaghi, Reticular synthesis of multinary covalent organic frameworks, J. Am. Chem. Soc. 141 (2019) 11420–11424.
[31] W. Chen, L. Wang, D. Mo, F. He, Z. Wen, X. Wu, H. Xu, L. Chen, Modulating benzothiadiazole-based covalent organic frameworks via halogenation for enhanced photocatalytic water splitting, Angew. Chem. Int. Ed. 59 (2020) 16902–16909.
[32] H. Cheng, H. Lv, J. Cheng, L. Wang, X. Wu, H. Xu, Rational design of covalent heptazine frameworks with spatially separated redox centers for high-efficiency photocatalytic hydrogen peroxide production, Adv. Mater. 34 (2022), e2107480.
[33] W.K. Han, Y. Liu, X. Yan, Y. Jiang, J. Zhang, Z.G. Gu, Integrating light-harvesting ruthenium(II)-based units into three-dimensional metal covalent organic frameworks for photocatalytic hydrogen evolution, Angew. Chem. Int. Ed. 61 (2022), e202208791.
[34] Y. Nosaka, A.Y. Nosaka, Generation and detection of reactive oxygen species in photocatalysis, Chem. Rev. 117 (2017) 11302–11336.
[35] W. Li, X. Huang, T. Zeng, Y.A. Liu, W. Hu, H. Yang, Y.B. Zhang, K. Wen, Thiazolo [5,4-d]thiazole-based donor-acceptor covalent organic framework for sunlight-driven hydrogen evolution, Angew. Chem. Int. Ed. 60 (2021) 1869–1874.
[36] C. Wu, Z. Teng, C. Yang, F. Chen, H.B. Yang, L. Wang, H. Xu, B. Liu, G. Zheng, Q. Han, Polarization engineering of covalent triazine frameworks for highly efficient photosynthesis of hydrogen peroxide from molecular oxygen and water, Adv. Mater. 34 (2022), e2110266.
[37] S. Fu, S. Yao, S. Guo, G.C. Guo, W. Yuan, T.B. Lu, Z.M. Zhang, Feeding carbonylation with CO_2 via the synergy of single-site/nanocluster catalysts in a photosensitizing MOF, J. Am. Chem. Soc. 143 (2021) 20792–20801.
[38] X. Zhang, P. Ma, C. Wang, L. Gan, X. Chen, P. Zhang, Y. Wang, H. Li, L. Wang, X. Zhou, K. Zheng, Unraveling the dual defect sites in graphite carbon nitride for ultra-high photocatalytic H_2O_2 evolution, Energy Environ. Sci. 15 (2022) 830–842.
[39] X. Zhang, J. Wang, B. Xiao, Y. Pu, Y. Yang, J. Geng, D. Wang, X. Chen, Y. Wei, K. Xiong, Y. Zhu, Resin-based photo-self-Fenton system with intensive mineralization by the synergistic effect of holes and hydroxyl radicals, Appl. Catal. B Environ. 315 (2022), 121525.
[40] C. Pan, G. Bian, Y. Zhang, Y. Lou, Y. Zhang, Y. Dong, J. Xu, Y. Zhu, Efficient and stable H_2O_2 production from H2O and O2 on BiPO4 photocatalyst, Appl. Catal. B Environ. 316 (2022), 121675.
[41] Z. Jiang, L. Wang, J. Lei, Y. Liu, J. Zhang, Photo-Fenton degradation of phenol by CdS/rGO/Fe^{2+} at natural pH with in situ-generated H_2O_2, Appl. Catal. B Environ. 241 (2019) 367–374.
[42] J. Ma, K. Wang, C. Wang, X. Chen, W. Zhu, G. Zhu, W. Yao, Y. Zhu, Photocatalysis-self-Fenton system with high-fluent degradation and high mineralization ability, Appl. Catal. B Environ. 276 (2020), 119150.
[43] F. Wang, J. Xu, Z. Wang, Y. Lou, C. Pan, Y. Zhu, Unprecedentedly efficient mineralization performance of photocatalysis-self-Fenton system towards organic pollutants over oxygen-doped porous g-C_3N_4 nanosheets, Appl. Catal. B Environ. 312 (2022), 121438.
[44] L. Chen, L. Wang, Y. Wan, Y. Zhang, Z. Qi, X. Wu, H. Xu, Acetylene and diacetylene functionalized covalent triazine frameworks as metal-free photocatalysts for hydrogen peroxide production: a new two-electron water oxidation pathway, Adv. Mater. 32 (2020), e1904433.
[45] H. Che, X. Gao, J. Chen, J. Hou, Y. Ao, P. Wang, Iodide-induced fragmentation of polymerized hydrophilic carbon nitride for high-performance quasi-homogeneous photocatalytic H_2O_2 production, Angew. Chem. Int. Ed. 60 (2021) 25546–25550.
[46] H. Koshima, K. Takechi, H. Uchimoto, M. Shiro, D. Hashizume, Photomechanical bending of salicylideneaniline crystals, Chem. Commun. 47 (2011) 11423–11425.
[47] Q. Zhi, W. Liu, R. Jiang, X. Zhan, Y. Jin, X. Chen, X. Yang, K. Wang, W. Cao, D. Qi, Piperazine-linked metalphthalocyanine frameworks for highly efficient visible-light-driven H_2O_2 photosynthesis, J. Am. Chem. Soc. 144 (2022) 21328–21336.
[48] J.A. Lannon, F.D. Verderame, R.W. Anderson Jr, Infrared spectrum of solid and matrix-isolated H_2O_2 and D_2O_2, J. Chem. Phys. 54 (1971) 2212–2223.
[49] J.-Y. Feng, Y.-P. Lee, H.A. Witek, T. Ebata, Vacuum ultraviolet photoionization induced proton migration and formation of a new C–N bond in pyridine clusters revealed by infrared spectroscopy and mass spectrometry, J. Phys. Chem. Lett. 12 (2021) 4936–4943.
[50] L. Wang, R. Lian, Y. Zhang, X. Ma, J. Huang, H. She, C. Liu, Q. Wang, Rational preparation of cocoon-like g-C_3N_4/COF hybrids: accelerated intramolecular charge delivery for photocatalytic hydrogen evolution, Appl. Catal. B Environ. 315 (2022), 121568.
[51] Y.J. Li, W.R. Cui, Q.Q. Jiang, Q. Wu, R.P. Liang, Q.X. Luo, J.D. Qiu, A general design approach toward covalent organic frameworks for highly efficient electrochemiluminescence, Nat. Commun. 12 (2021) 4735.